

## Level Structure of the Low-Lying Excited States of $^{116}\text{Sn}$ Populated by the Radiative Capture of Thermal Neutrons\*

D. A. McClure and J. W. Lewis, III†  
*Georgia Institute of Technology, Atlanta, Georgia 30332*  
 (Received 1 October 1971)

The low-lying excited states of  $^{116}\text{Sn}$  populated by primary and secondary  $\gamma$ -ray transitions from the reaction  $^{115}\text{Sn}(n, \gamma)^{116}\text{Sn}$  were studied. Both singles and  $\gamma$ - $\gamma$  coincidence techniques were employed with the exclusive use of Ge(Li) detectors. Results obtained from high-energy  $\gamma$ -ray spectra ( $\sim 5.9$ – $10$  MeV) were combined with those from low-energy singles spectra ( $\sim 100$  keV– $3.8$  MeV) and low-low coincidence spectra in order to infer the excitation energies and branching characteristics of 21 states up to an energy of  $\sim 3.7$  keV. A level and decay scheme is proposed including a total of 45  $\gamma$  rays representing  $\sim 90\%$  of the decay intensity. This scheme includes most of the levels having  $E_x \leq 3$  MeV which were observed previously in charged-particle reactions and  $\beta$ -decay studies. The existence of the  $0^+$  level having an excitation energy of 2027 keV has been confirmed and a new level at 2545-keV excitation is proposed.

### I. INTRODUCTION

The even-even tin isotopes have been the subject of a large number of experimental and theoretical investigations in recent years.<sup>1-17</sup> The existing experimental data have been summarized by Beer *et al.*,<sup>9</sup> and a review of both the theoretical and experimental results has been presented by Baranger.<sup>13</sup>

The tin isotopes are single closed-shell nuclides ( $Z=50$ ) and thus any differences in nuclear structure will be determined completely by the differences in the numbers of neutrons present in the outer shells. According to the simple shell model the valence neutrons will be distributed between the  $2d_{5/2}$ ,  $1g_{7/2}$ ,  $3s_{1/2}$ ,  $2d_{3/2}$ , and  $1h_{11/2}$  levels. The tin isotopes are, therefore, far from a closed neutron shell. The  $^{116}\text{Sn}_{66}$  nucleus has the neutron shells filled up through the  $3s_{1/2}$  level and exhibits accordingly the qualitative features of a collective motion which is vibrational in nature.

The theoretical calculations have involved the use of the BCS quasiparticle model including various residual forces such as the pairing-plus-quadrupole interaction<sup>14</sup> and Gaussian-shaped potentials.<sup>15</sup> Recent work by at least two groups has employed the quasiparticle theory with so-called realistic residual interaction forces.<sup>16, 17</sup> The calculations have recently met with some degree of success in the description of many of the low-lying levels in the  $^{116}\text{Sn}$  nuclide ( $E_x \leq 3$  MeV).

In spite of the wealth of experimental information available concerning  $^{116}\text{Sn}_{66}$  there remained several ambiguities in the proposed level schemes. The thermal-neutron-capture reaction is unencumbered by the selection rules involved in

charged-particle and  $\beta$ -decay studies and is, therefore, capable of populating virtually every low-lying excited state in a product nucleus.<sup>18</sup> For this reason it was felt that a comprehensive re-examination of the levels of this nuclide using the  $(n, \gamma)$  reaction might provide additional or more-detailed information concerning these states. In particular the precise determination of the energies and branching ratios of these levels should aid in the understanding of the low-lying levels of this nuclide.

The present paper describes the results of an investigation of the low-lying excited states of  $^{116}\text{Sn}_{66}$  populated by the radiative capture of thermal neutrons in  $^{115}\text{Sn}$ .<sup>19</sup> Both singles and coincidence spectroscopic techniques have been employed with the exclusive use of Ge(Li) detectors. The studies included coincidence data involving the high-energy ( $\sim 6$ – $10$ -MeV) primary  $\gamma$ -ray transitions and the low-energy ( $\sim 100$ -keV– $4$ -MeV) transitions, as well as coincidences between the low-energy  $\gamma$ -ray cascades.

### II. EXPERIMENTAL FACILITY AND APPARATUS

#### A. External Beam Facility

Figure 1 shows a diagram of the external beam facility which consists of the beam-port interior to the reactor and the external shielding and target cave. The beam port is a 15-cm-diam tangential through tube in the Georgia Institute of Technology research reactor. The tube passes completely through the reactor and its center is adjacent to one of the fuel elements. There is no straight-line path from the core of the reactor to

the external target chamber, thus eliminating a source of background  $\gamma$  radiation.

An increase in the thermal-neutron flux in the external beam was obtained by placing a 30-cm-long by 15-cm-diam section of reactor-grade graphite at the center of the through tube. This graphite block was positioned so that its front face was at the center of the through tube adjacent to a fuel element. Two graphite plugs were placed in the through tube, one in front of and one behind the graphite block. Each plug was approximately 1.3 m long and 15 cm in diam with a 2-cm-diam hole in the center. The front section increased the external thermal-neutron flux by approximately 15%, while the section behind the graphite block had virtually no effect on the external neutron flux.

The remaining 2 m of the through tube contains the final collimating plug. The outer coaxial portion of this plug consists of dense concrete interspersed with iron punchings. The inner portion of the plug (beginning at the point nearest the reactor core) is filled with polyethylene (impregnated with 2% boron) with a 1.25-cm-diam hole in its center. The final collimator consists of four 4.5-cm-long steel plugs with tapered holes which serve to remove the  $\gamma$  radiation resulting from neutron capture in any of the internal materials while at the same time serving to sharpen the edges of the beam by minimizing the low-angle neutron scattering.

The considerable background  $\gamma$  radiation in the beam has been removed by the insertion of a 7-cm by 1.25-cm-diam bismuth single crystal into the neutron beam at the location shown in Fig. 1. The

bismuth crystal has a higher scattering cross section for fast neutrons than for thermal neutrons and thus also serves to improve the cadmium ratio of the beam. The external neutron beam at the target position is characterized by a thermal-neutron flux of  $\sim 4 \times 10^6$  n/cm<sup>2</sup>sec and a cadmium ratio of  $\sim 80$ .

Final collimation is provided at the entrance to the target cave by a 4.5-cm-diam <sup>6</sup>LiF disk having a 1.25-cm-diam center hole. In this way any neutrons which may have undergone low-angle scattering are prevented from entering the cave and the detectors. A similar disk guards the exit of the cave. The cave itself consists of a minimum of 3 cm of lead shielding and effectively prevents room background  $\gamma$  radiation from reaching the detectors.

#### B. Electronic Apparatus

The outputs of two lithium-drifted germanium detectors are each amplified and addressed to analog-to-digital converters (ADC) by conventional pulse amplifying and shaping circuits (Fig. 2). The analog electronics were constructed from diagrams supplied by the electronics group at Argonne National Laboratory.<sup>20</sup> The following options are available for application to the analog signals: (1) pole-zero cancellation, (2) dc restoration, (3) pulse-shape discrimination, and (4) artificial dead-time insertion. The net result is that high counting rates can be accommodated with a minimum loss in the intrinsic resolution capability of the Ge(Li) detectors. The output from

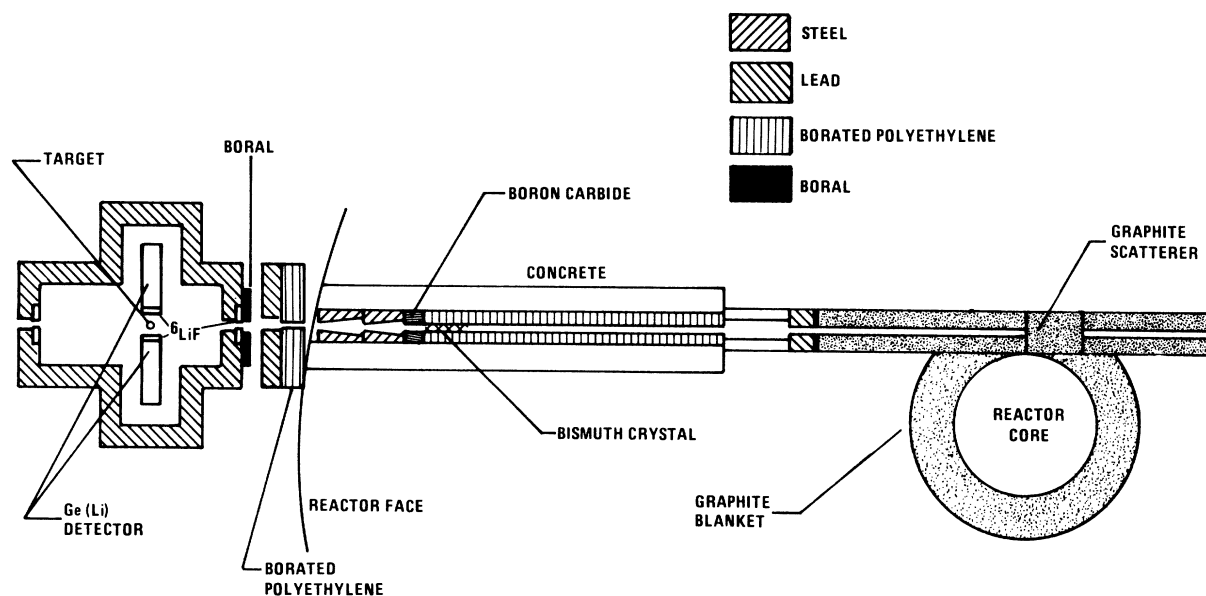


FIG. 1. Representation of the external-neutron-beam facility and target cave (not to scale).

the ADC's is stored either in a magnetic-core memory (singles spectra) or on magnetic tape (coincidence studies).

Digital zero and gain stabilization was employed throughout the lengthy time required to collect the coincidence data. Stabilization was based on the output of two highly stable dual pulsers,<sup>20</sup> one for each arm of the coincidence system. A "tag" output from the dual pulsers assured that the stabilizer operated only on the pulser output and allowed the pulser pulses to be rejected for storage on the magnetic tape.

The  $\gamma$ - $\gamma$  coincidence data were stored on magnetic tape using an ADC to magnetic tape drive interface designed and constructed at Georgia Institute of Technology.<sup>21</sup> This system allows the storage of one-, two-, or three-parameter coincidence events and has been designed to allow the storage of two 4096-channel energy spectra and the corresponding time spectrum. The system was used in the two-parameter mode for this particular series of studies.

An 8192-channel ADC was employed in each arm of the coincidence system. For the work

described here 2048-channel sections of the spectrum were selected for storage. The data were stored in address pairs on computer-compatible magnetic tape which was equivalent to performing a two-parameter investigation with a  $2048 \times 2048$ -channel memory. Each tape held a storage capacity of  $\sim 3 \times 10^6$  address-pair events.

A time-to-amplitude converter served as the basis of the fast-timing circuitry. The output signal of a single-channel analyzer was set on either the prompt time distribution (true coincidence events) or the chance portion of the time spectrum. However, the true-to-chance ratio was always greater than 10, so that chance contributions were always negligible in the resulting  $\gamma$ -ray coincidence spectra.

### III. RESULTS

#### A. High-Energy Transitions

The singles spectrum representing the primary high-energy capture  $\gamma$  rays from the reaction  $^{115}\text{Sn}(n, \gamma)^{116}\text{Sn}$  is presented in Fig. 3. The energies of several peaks are given on the figure as

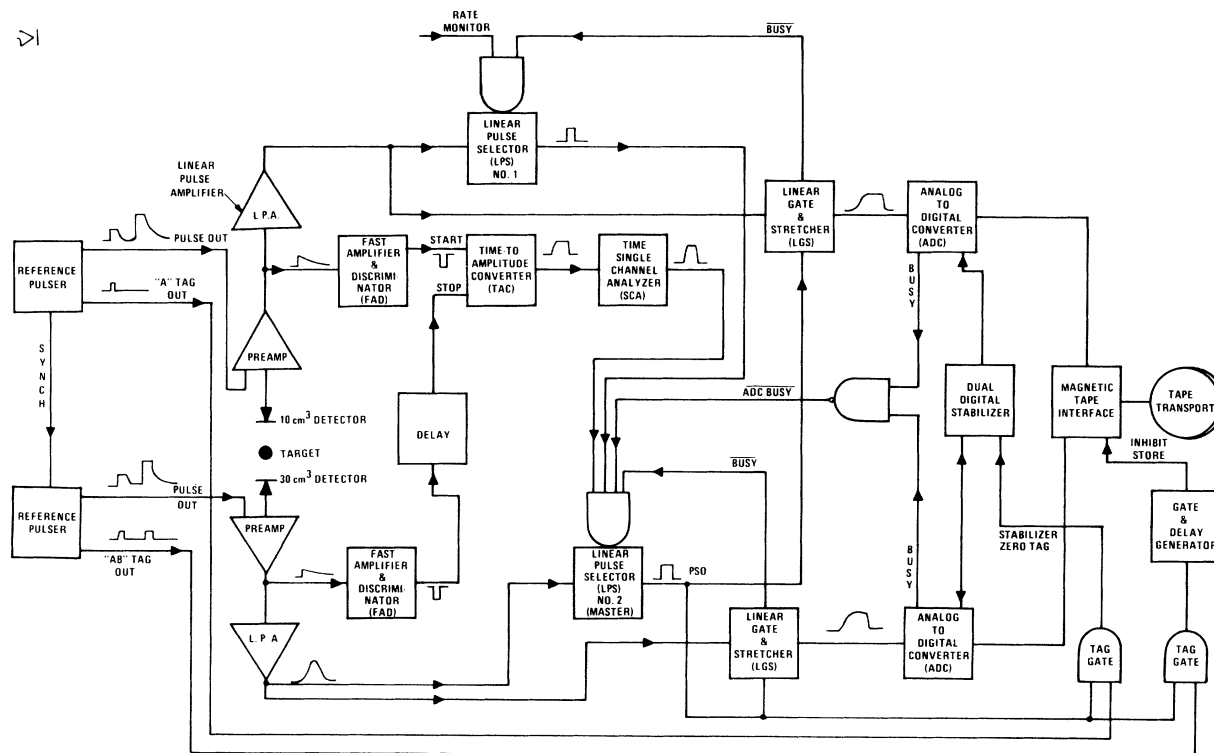


FIG. 2. Schematic representation of the electronic circuitry. Both detectors were characterized by a full width at half maximum of  $\sim 4.5$  keV at 1.3 MeV. The  $10\text{-cm}^3$  detector was used for the singles investigations because of its superior peak shape. Coincidence data were taken in the two-parameter mode utilizing digital zero and gain stabilization in both arms of the system. Stabilization was based on the use of two dual pulsers and the stabilization peaks were not stored on the magnetic tape.

a guide. Those peaks marked with a C denote contaminant background radiation. It can be seen that three peaks were observed for most of the transitions; corresponding to the escape of zero, one, or both of the annihilation quanta. The so-called double-escape (DE) peak is the most intense in this energy region, and therefore the energies and intensities of the transitions are based mainly on the location and area of this peak. The assignment of DE peaks was corroborated by a pair spectrometer spectrum (which records only the DE peaks) which included the same energy region.

The energies of the  $\gamma$  rays in the spectrum were determined by a comparison with the  $\gamma$  rays resulting from capture in  $^{14}\text{N}$ .<sup>22</sup> Correction for nonlinearities, which were present in the analog amplification and shaping circuitry, were deduced by using a highly linear voltage ramp generator. The output from the ramp generator was chopped and addressed to the test input of the preamplifier. In this manner any nonlinearities in the entire analog signal-amplification chain were uncovered.<sup>23</sup> Three spectra were recorded for each energy region of interest: (1) the  $\gamma$  rays resulting from capture in natural nitrogen (melamine target),

(2) the spectrum from radiative capture in  $^{115}\text{Sn}$ , and (3) the ramp spectrum. The peaks in both  $\gamma$ -ray spectra were fitted using a Gaussian function for the peak shape.<sup>24</sup> The resulting centroids and areas were used in the calculation of the energies and intensities of the various transitions. Figure 4 shows the DE-peak efficiency curve derived from the known intensities in the nitrogen spectrum. This curve was used to calculate the relative intensities of the high-energy  $\gamma$ -ray transitions observed in  $^{116}\text{Sn}$ .

The energies of the primary transitions, i.e.,  $\gamma$  rays which proceed directly from the capture state to one of the low-lying excited states, have been defined by using the usual, well-founded assumption that in this mass region  $\gamma$  rays which have energies  $\geq 70\%$  of the neutron binding energy are primary transitions. The neutron binding energy was determined to be  $9562 \pm 1.5$  keV from the energy of the observed primary transition to the ground state (the fact that this  $\gamma$  ray was not observed in the coincidence studies supports its placement as the ground-state transition). This value for the binding energy deviates from the value of  $9.43 \pm 0.08$  MeV determined from previous ( $n, \gamma$ ) investigations.<sup>25</sup> However, it is in excellent

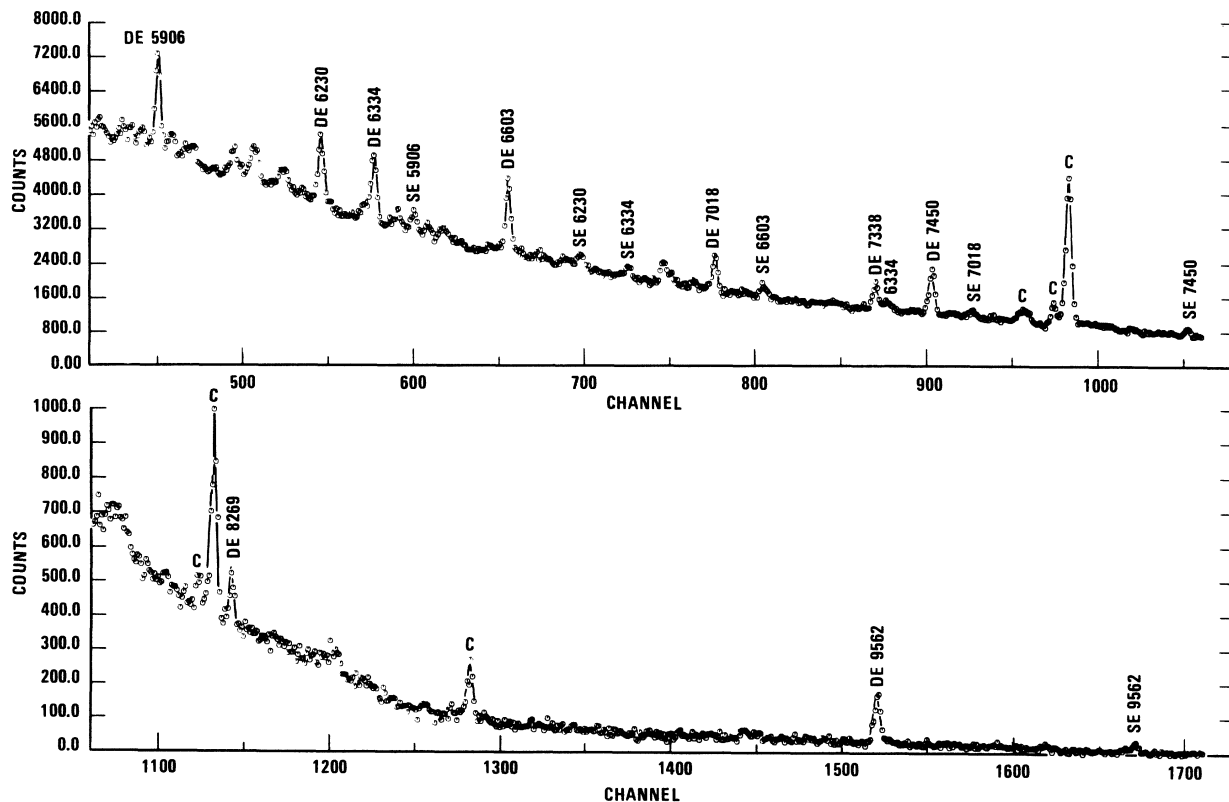


FIG. 3. Representative high-energy pulse-height spectrum. Single-escape and double-escape peaks are labeled (SE) and (DE), respectively. Peaks labeled C are due to contaminant background radiation.

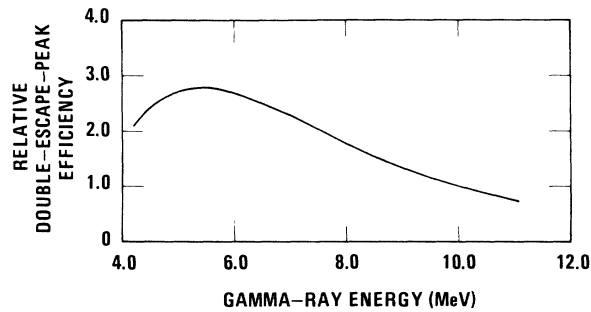


FIG. 4. Empirically determined relative double-escape-peak efficiency of the Ge(Li) system as a function of the  $\gamma$ -ray energy.

TABLE I. Primary  $\gamma$ -ray transitions.

Energy (keV)	Relative intensity <sup>a</sup>	Low-lying level
$9562 \pm 1.5$	22	0
$8269 \pm 1.5$	11	1293
$7450 \pm 1.5$	76	2112
$7338 \pm 1.5$	47	2224
$7018 \pm 1.5$	50	2544
$6603 \pm 1.5$	100	2959
$6333 \pm 1.5^b$	98	3229
$6229 \pm 1.5^b$	94	3333
$5904 \pm 1.5^b$	91	3658

<sup>a</sup> Associated errors are  $\pm 15\%$ .

<sup>b</sup> May not be a primary transition.

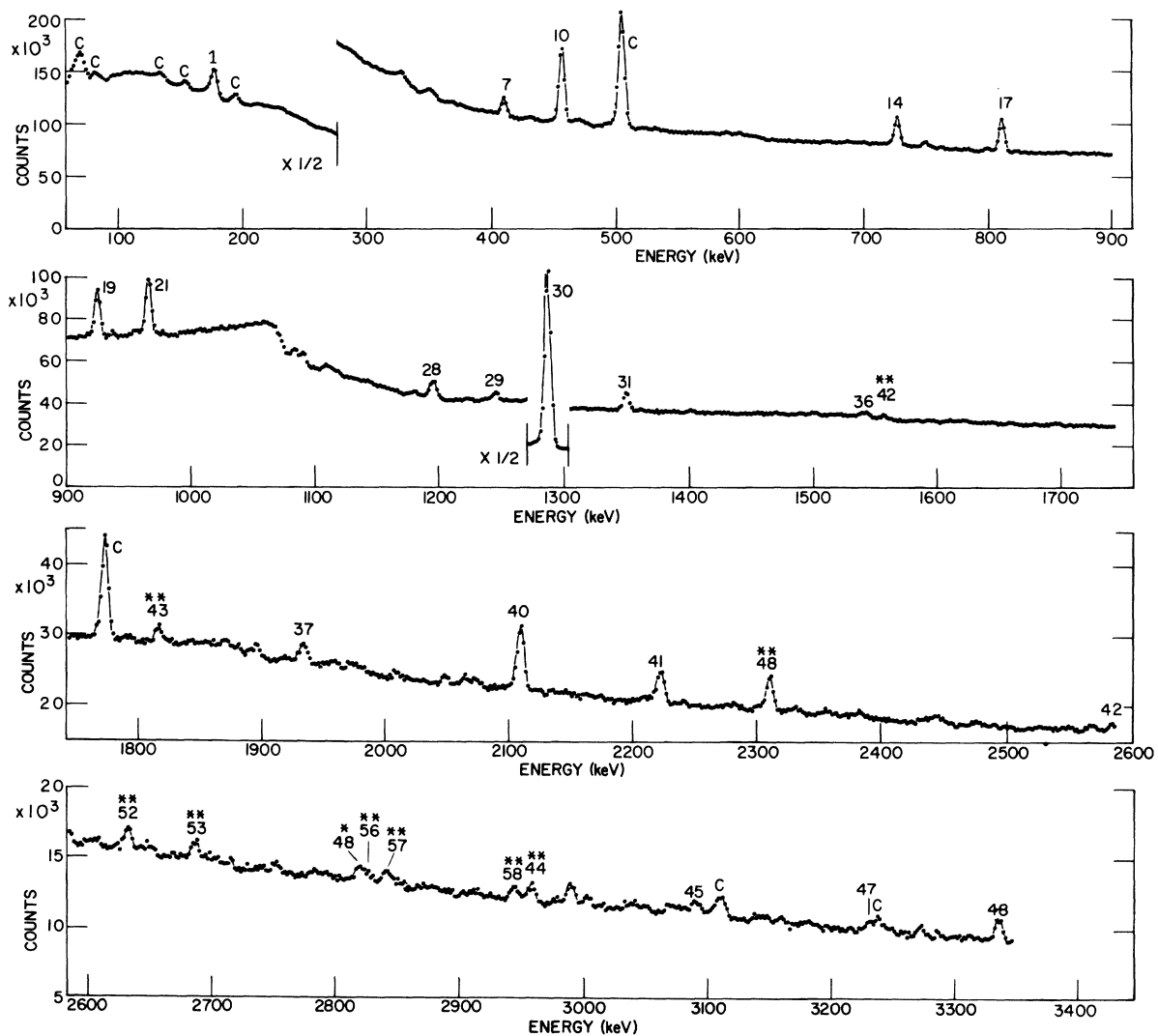


FIG. 5. Representative portions of the low-energy pulse-height spectrum obtained for the reaction  $^{115}\text{Sn}(n, \gamma)^{116}\text{Sn}$ . Those peaks labeled C are due to contaminant background radiation. Single-escape and double-escape peaks are labeled with \* and \*\*, respectively. The numbers appearing with some peaks correspond to the list of low-energy  $\gamma$  rays given in Table II.

agreement with the value of  $9563 \pm 1$  keV calculated from the mass-difference tables.<sup>26</sup>

A summary of the high-energy transitions is presented in Table I. Those transitions which do not conform to the conservative and somewhat arbitrary definition of a primary transition have been indicated in Table I. However, these transitions seem to populate levels which were observed in  $(d, p)^{10}$  or  $(p, p')^{6-9}$  reactions and are included in the event that later evidence supports their placement as primary transitions.

A coincidence study was performed involving the high-energy transitions (5–10 MeV) in one arm of the coincidence system and the low-energy transitions (~60 keV to 3.7 MeV) in the other arm. Unfortunately these data are of poor statistical quality owing primarily to the poor peak-height-to-background ratio and no new information resulted from this study. In retrospect it is perhaps obvious that this would be the case for the following reasons. The ground-state spin and parity of  $^{115}\text{Sn}$  are  $\frac{1}{2}^+$ .<sup>27</sup> Therefore, the compound-nuclear state produced in the thermal-neutron-capture reaction (*s*-wave capture) can be repre-

sented by a mixture of states dominated by spin and parity  $0^+$  and  $1^+$ . The most intense radiation resulting from neutron capture is usually of *E1* multipolarity.<sup>18</sup> However, the low-energy excited states in  $^{116}\text{Sn}$  are primarily  $0^+$ ,  $2^+$ , and  $4^+$ . Therefore, primary  $\gamma$ -ray transitions to these states must involve at least *E2* multipolarity. For this reason a major portion of the primary radiation is expected to proceed from the capture state through the multitude of levels at intermediate energy (2–7 MeV) where transitions having *E1* multipolarity would be allowed. This fact implies that the low-lying levels would be weakly populated by primary radiation but could be strongly populated via cascade  $\gamma$ -ray transitions involving the intermediate levels.

#### B. Low-Energy Transitions

The spectrum of the low-energy transitions resulting from the reaction  $^{115}\text{Sn}(n, \gamma)^{116}\text{Sn}$  is shown in Fig. 5. The numbers on the figure correspond to the list of low-energy  $\gamma$  rays given in Table II. DE and single-escape (SE) peaks are represented

TABLE II. Low-energy  $\gamma$ -ray transitions.

Energy (keV)	Relative intensity	Assignment (keV)	Energy (keV)	Relative intensity	Assignment (keV)
179.5 ± 0.3	0.40		1293.5 ± 0.3	100 <sup>a</sup>	1293-0
329.2 ± 0.3	0.22		1356.6 ± 0.3	5.4 <sup>a</sup>	2649-1293
334.1 ± 0.3	0.67		1408.6 ± 0.3	0.46	2701-1293
355.0 ± 0.3	0.49	2112-1757	1496.8 ± 0.3	0.51	
359.6 ± 0.3	0.34		1507.8 ± 0.3	0.94	2801-1293
374.1 ± 0.3	0.23	3334-2959	1545.9 ± 0.3	1.1	3658-2112
416.7 ± 0.3	1.6 <sup>a</sup>	2528-2112	1550.8 ± 0.3	1.5	2844-1293
435.4 ± 0.3	0.13	2701-2266	1935.5 ± 0.5	0.68	3230-1293
439.1 ± 0.3	0.22	3089-2650	2021.7 ± 0.5	0.36	
463.4 ± 0.3	9.0 <sup>a</sup>	1757-1293	2051.3 ± 0.5	1.6	
476.9 ± 0.3	0.65	2701-2225	2112.2 ± 0.5	13.8 <sup>a</sup>	2112-0
500.0 ± 0.3	0.38		2224.7 ± 0.5	7.7 <sup>a</sup>	2224-0
506.2 ± 0.3	1.0		2586.3 ± 0.5	3.2	2586-0
733.8 ± 0.3	6.4 <sup>a</sup>	2027-1293	2843.5 ± 0.5	2.1	2543-0
769.1 ± 0.3	0.18		2960.5 ± 0.5	2.0	2959-0
806.7 ± 0.3	0.94	3334-2528	3089.4 ± 1.0	2.8	3089-0
818.1 ± 0.3	8.7 <sup>a</sup>	2112-1293	3097.2 ± 1.0	1.1	
830.1 ± 0.3	0.41	2586-1756	3231.0 ± 1.2	1.6	3230-0
931.8 ± 0.3	7.3 <sup>a</sup>	2224-1293	3334.2 ± 1.2	4.0	3334-0
962.4 ± 0.3	1.2	3230-2266	3405.4 ± 1.5	2.0	3405-0
972.6 ± 0.3	10.6 <sup>a</sup>	2266-1293	3454.9 ± 1.5	2.2	3455-0
1096.9 ± 0.3	1.6	2390-1293	3499.8 ± 1.5	0.9	
1114.9 ± 0.3	1.2		3658.5 ± 1.5	2.2	3658-0
1119.5 ± 0.3	0.91	3230-2112	3712.4 ± 1.5	1.7	
1124.8 ± 0.3	0.71		3777.3 ± 1.5	1.0	
1187.0 ± 0.3	0.70	3453-2266	3809.1 ± 1.5	0.7	
1199.6 ± 0.3	1.7		3853.7 ± 1.5	0.7	
1202.9 ± 0.3	1.8	3230-2027	3869.3 ± 1.5	0.8	
1251.9 ± 0.3	2.1 <sup>a</sup>	2544-1293	3968.0 ± 1.5	1.6	

<sup>a</sup> Error ±10%, error ±≤25% for other peaks.

in Fig. 5 by \*\* and \*, respectively. The energies were determined using the ramp method discussed in Sec. III A. The 511-keV transition resulting from the annihilation quanta and the 1778.7-keV transition resulting from the decay of  $^{28}\text{Al}$  (which was present as background radiation) were used as energy standards. A set of absolute intensity calibration sources (International Atomic Energy Agency, Vienna, Austria, 1969) served to define the efficiency curve up to 1.33 MeV. This curve was extended to 4 MeV by observing the spectrum from a melamine target ( $^{15}\text{N}$ ) for which the relative intensities of lines in this energy region are well known.<sup>22</sup> Coincidence relationships between the low-energy (100-keV–4-MeV) transitions were recorded in a  $2048 \times 2048$ -channel array on computer-compatible magnetic tape. The results of this study are presented in Table III.

The left-hand column represents the energy of the  $\gamma$ -ray transition which was used as a gate while searching the magnetic-tape data. The right-hand column includes the energies of the transitions which were observed in the resulting coincidence spectrum. Those energies followed by (?) indicate a less certain coincidence assignment and should not be considered unambiguous. Figure 6 shows some representative coincidence spectra. The upper entry [Fig. 6(a)] depicts the singles spectrum. The coincidence spectra [Figs. 6(b)–6(d)] have been corrected for events involving the relatively large underlying Compton distribution. The vertical lines in the coincidence spectra correspond to 1 standard deviation.

#### IV. LEVEL SCHEME

The results of the high-energy primary  $\gamma$ -ray study listed in Table I have established the positions of five excited states up to 2959 keV. Figure

7 shows the excited states up to an energy of  $\sim 3700$  keV which were observed in this study. States which have been observed in the various charged-particle studies<sup>6–11</sup> are indicated schematically by downward-pointing flags on the right. The energies of these states have been corroborated and more definitely established from the energies of the primary and secondary thermal-neutron-capture  $\gamma$  rays. Levels which have been previously observed in  $\beta$ -decay studies<sup>1–5</sup> have been indicated in Fig. 7 by downward-pointing flags on the left. Those transitions which were observed in the coincidence studies have been indicated by a dot at the initiating level and/or the terminating level.

The primary  $\gamma$ -ray transitions are observed not to terminate at all of the levels reported in the  $(d, p)$  studies,<sup>10</sup> as expected. There also is no apparent correlation between the intensities of the primary  $\gamma$  rays and the population strengths of the low-lying levels in the  $(d, p)$  reaction.

When the low-energy singles data (Table II) and the summary of the low-low coincidence studies (Table III) were combined with the results of the primary high-energy  $\gamma$ -ray investigation, the existence of several states which were not populated by the primary  $\gamma$  rays was detected. These additional states and the intervening  $\gamma$ -ray transitions have been reliably and unambiguously placed in the proposed level scheme.

It should be noted that with the exception of the relatively high-energy, high-spin states (i.e., the  $5^-$  level at 2367 keV and the  $7^-$  level at 2890 keV), which are not expected to be populated by the  $(n, \gamma)$  reaction, every state observed in the charged-particle and  $\beta$ -decay studies is also present in the  $(n, \gamma)$  investigation. Some question still remains as to the exact correspondence between the present levels and previously defined levels be-

TABLE III. Coincidence relationships.

Transition energy (keV)	Observed coincidence transition energy (keV)
357	463, 1293
417	818, 1293
463	357(?), <sup>a</sup> 1293
734	1202, 1293
818	1293
932	1293
972	1293
1202	1293
1293	417, 463, 734, 818, 932, 972, 1097(?), 1202, 1252, 1356
1356	1293
1935	1293(?)

<sup>a</sup> Transitions followed by (?) are less confidently assigned and should not be considered as completely unambiguous.

cause of small but possibly significant energy mismatches. The present studies also serve to define several levels which were unobserved (or observed only weakly) in the charged-particle and

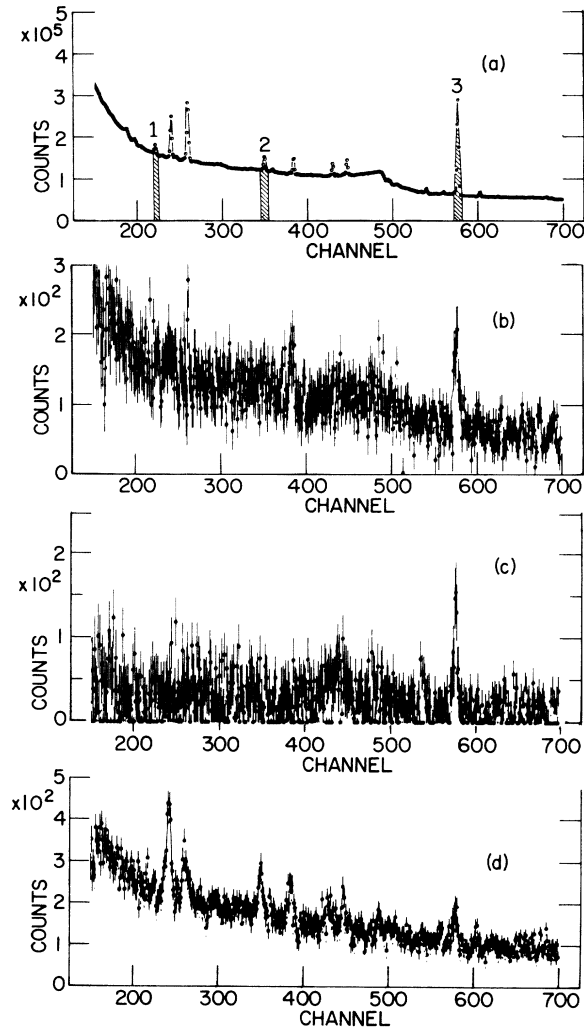


FIG. 6. Typical portions of the low-energy spectra in coincidence with particular low-energy coincidence gates specified by the numbered and cross-hatched peaks of the singles spectrum shown in the upper portion of the figure [part (a)]. The three lower coincidence spectra [parts (b)–(d)] correspond to gates 1 (417 keV), 2 (734 keV), and 3 (1293 keV), respectively. The three lower spectra have been corrected for the underlying Compton events but have not been corrected for chance coincidence events. The chance contribution can be estimated by comparing the singles spectrum (which has the shape of the chance contribution) and the magnitude of the “self-coincident” peak at 1293 keV in part (d) [spectrum (d) should contain the largest chance contribution of any coincidence spectrum, since it represents coincidence events with the most intense transition in the singles spectrum].

$\beta$ -decay investigations.

For example, the 734-keV transition to the first excited state at 1293 keV delineates the existence of a level at 2027.3 keV which has been unobserved in recent  $\beta$ -decay<sup>2</sup> and  $(p, p')$ <sup>9</sup> studies, but was observed weakly in previous  $(p, p')$ ,  $(p, d)$ , and  $(d, p)$  studies.<sup>6–8</sup> In addition, the energy of this level has been accurately determined and its branching characteristics unambiguously defined for the first time in this study. The 7018-keV primary transition defines a level at 2545.4-keV excitation. This level was probably unobserved in previous studies, although an energy mismatch allows that it may have been observed in the  $(p, d)$  work of Yagi *et al.*<sup>8</sup>

Several of the transitions observed in the singles  $\gamma$ -ray spectrum were too weak to be seen in the coincidence studies. A few of these transitions have been included in the decay scheme shown in Fig. 7 on the basis of energy and intensity balances alone. These transitions and the corresponding excited states are considered to be less well established than those supported by the coincidence studies.

## V. DISCUSSION

In the usual case the primary  $\gamma$  rays resulting from the radiative capture of thermal neutrons have intensities which are a decreasing function of the multipolarity of the transition; i.e.,  $E1$  radiation is most intense and  $E2, M1$  radiation is relatively weak if it is observed at all. However, the lowest-lying levels of  $^{116}\text{Sn}$  are expected to have spin and parity of  $(0, 2, 4)^+$ .<sup>13</sup> Therefore, primary radiation populating these lowest-lying levels must be of  $E2, M1$  multipolarity. For this reason the relatively weak population of the ground state and the first excited state at 1293.5 keV by primary  $\gamma$  radiation is consistent with the previous spin and parity assignments<sup>1–12</sup> of  $0^+$  and  $2^+$ , respectively. The 1756.9-keV state has been assigned spin and parity of  $0^+$  in the  $\beta$ -decay,<sup>1–5</sup>  $(p, t)$ ,<sup>8</sup> and  $(d, p)$ <sup>10</sup> studies. This state was observed to decay solely to the  $2^+$  state at 1293 keV in this study. The fact that there was no observable transition to the  $0^+$  ground state from the 1756.9-keV level is consistent with the  $0^+$  assignment (the absence of a primary transition to this level is not significant in view of the Porter-Thomas<sup>18</sup> distribution of radiation widths).

The existence of the level at 2027.3-keV excitation energy has been indicated previously by the older  $(p, p')$ ,  $(p, d)$ ,  $(p, t)$ ,  $(d, p)$ ,<sup>6–8</sup> and  $\beta$ -decay<sup>1–4</sup> studies; however, it has remained unobserved in more recent  $(p, p')$ <sup>9</sup> and  $\beta$ -decay<sup>2</sup> investigations. The decay of this level to the  $2^+$  first excited state and the notable absence of transitions from this



level to the ground state or to the 1756.9-keV level support the  $0^+$  assignment. The energy and  $\gamma$ -ray branching of this level have been unambiguously defined in this study.

The level at 2111.8 keV has been observed previously<sup>1-12</sup> and both the primary ( $n, \gamma$ ) population of this level and its subsequent decay characteristics support the previous  $2^+$  assignment. The 2225.0-keV level has been observed previously<sup>1-12</sup> and has been assigned spin and parity  $2^+$ . The population of the 2225.0-keV level by primary radiation and its subsequent decay to  $0^+$  and  $2^+$  levels support this assignment. The 2266.1-keV state is probably the collective  $3^-$  level due pri-

marily to core excitation.<sup>13</sup> The decay of this level is consistent with a  $3^-$  assignment.

The 2390.4-keV level was not populated by primary ( $n, \gamma$ ) radiation and is only weakly observed in the coincidence studies. This level is, therefore, less well defined than in previous  $\beta$ -decay<sup>1-4</sup> investigations. The decay properties of the level at 2528.5-keV excitation are consistent with the previous<sup>10</sup>  $4^+$  assignment.

The level at 2545.4-keV excitation energy was populated by primary radiation which limits its spin to 0, 1, 2, 3 if population by either  $E1$  or  $E2-M1$  radiation is considered. An ambiguity exists in the comparison of the energy of this level to

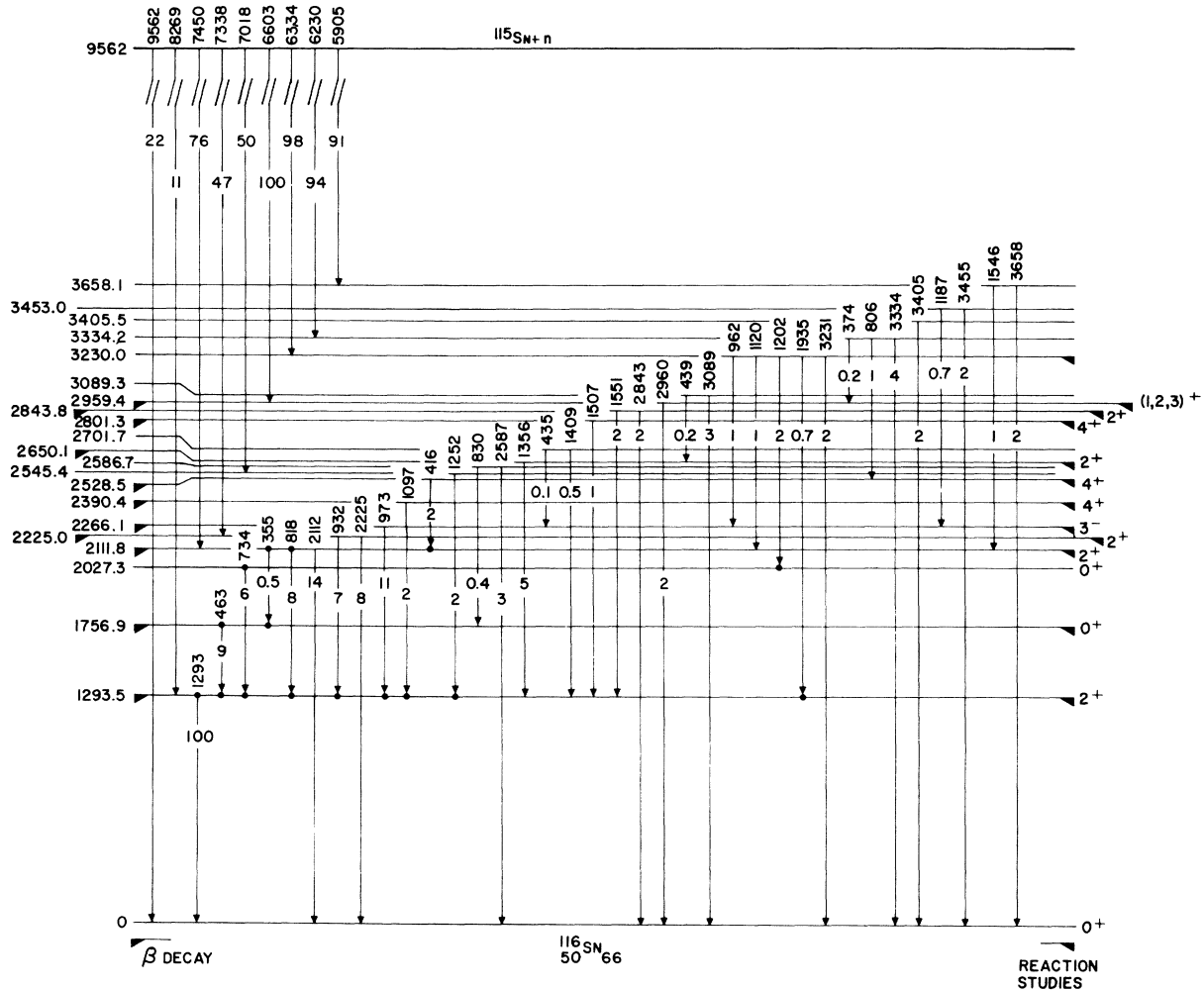


FIG. 7. Proposed level scheme of  $^{116}\text{Sn}$  deduced from the various coincidence and singles  $\gamma$ -ray investigations of the present work. The excitation energies are given in keV. Those levels marked on the left by downward-pointing flags correspond to levels observed in previous  $\beta$ -decay studies. Those levels marked with flags on the right are associated with reported charged-particle-reaction populations.  $\gamma$ -ray energies are in keV. Low-energy  $\gamma$ -ray intensities are relative to the intensity of the 1293-keV transition, and high-energy  $\gamma$ -ray intensities are relative to the intensity of the 6603-keV transition. Transitions designated by a dot at the initiation or termination of a  $\gamma$ -ray line have been observed in the coincidence studies. The spins and parities shown here are due mainly to previous assignments from  $\beta$ -decay and charged-particle investigations.

the levels observed in the charged-particle reactions. However, the possible candidates for the corresponding level in these studies have been assigned  $4^+$ . It is, therefore, most likely that this level has not been observed previously and represents a new level having  $J^\pi$  of either  $(0, 1, 2)^-$  or  $(0, 1, 2, 3)^+$ .

12 levels have been shown with an excitation energy greater than 2550 keV. The spin assignments (if shown) are those of previous investigators.<sup>9</sup> The placement of these states is less certain than those states which have been mentioned previously. Those levels which have been populated by primary radiation or observed in the coincidence studies are more definitely placed than the levels which are based only on energy and intensity balances.

In recent years it has become fashionable to describe the levels of  $^{116}\text{Sn}$  in terms of the BCS quasiparticle theory using various realistic interaction forces (the discussion of this nuclide in terms of the vibrational model has virtually disappeared in recent work). A discussion of the existing calculations and experimental results has been presented by Baranger.<sup>13</sup> The theory has recently met with some success in the description of the properties of the even-even nuclides in this

region by using a two-quasiparticle description of the low-lying excited states. The positions and decay properties of the  $2^+$  and  $3^-$  collective states (i.e., the 1293-, 2112-, 2225-, and 2266-keV levels of  $^{116}\text{Sn}$ ) have been characterized quite well by these calculations. However, there are more experimental than theoretical levels having spin and parity  $0^+$ ,  $2^+$ , and  $4^+$ .

## VI. ACKNOWLEDGMENTS

The authors gratefully acknowledge the help of H. H. Bolotin and S. B. Burson of Argonne National Laboratory for discussions concerning the beam-port facility. We are indebted to M. G. Strauss of Argonne for supplying circuit diagrams for most of the analog electronic circuitry, and to J. M. Palms at Emory University for the construction of a Ge(Li) detector used in this experiment. We are indebted to the nuclear group at the Georgia Institute of Technology for many helpful discussions; especially to N. S. Kendrick for the design and construction of the three-parameter magnetic-tape system and to C. H. Braden for suggestions concerning the manuscript. We thank the staff of the Georgia Institute of Technology research reactor for their cooperation.

\*Work supported in part by the National Science Foundation.

<sup>1</sup>Includes work performed for partial fulfillment of the Ph.D. dissertation requirements, Georgia Institute of Technology, 1971.

<sup>2</sup>J. Kantele and M. Karras, *Phys. Rev.* **135**, B9 (1964).

<sup>3</sup>E. Bodenstedt *et al.*, *Nucl. Phys.* **89**, 305 (1966).

<sup>4</sup>H. Ikegami and T. Udagawa, *Phys. Rev.* **124**, 1518 (1961).

<sup>5</sup>H. H. Bolotin, A. C. Lie, and A. Schwarzschild, *Phys. Rev.* **124**, 213 (1961); H. H. Bolotin, *ibid.* **136**, B1557, B1566 (1964).

<sup>6</sup>P. Fettweis and J. Vervier, *Phys. Letters* **3**, 36 (1962).

<sup>7</sup>D. L. Allan, B. H. Armitage, and B. A. Doran, *Nucl. Phys.* **66**, 481 (1965).

<sup>8</sup>E. J. Schneid, E. W. Hamburger, and B. L. Cohen, *Phys. Rev.* **161**, 1208 (1967).

<sup>9</sup>K. Yagi, Y. Saji, T. Ishimatsu, Y. Ishizaki, M. Motoba, Y. Nakajima, and C. Y. Huang, *Nucl. Phys.* **A111**, 129 (1968).

<sup>10</sup>O. Beer, A. E. Behay, P. Lopato, Y. Terrien, G. Vallois, and K. K. Seth, *Nucl. Phys.* **A147**, 326 (1970).

<sup>11</sup>E. J. Schneid, A. Prakash, and B. L. Cohen, *Phys. Rev.* **156**, 1316 (1967).

<sup>12</sup>T. Yamazaki and G. T. Ewan, *Nucl. Phys.* **A134**, 81 (1969); Ch. Chang, G. B. Hageman, and T. Yamazaki, *ibid.* **A134**, 110 (1969).

<sup>13</sup>D. G. Fleming, M. Blann, H. W. Fulbright, and J. A. Robbins, *Nucl. Phys.* **A157**, 1 (1970).

<sup>14</sup>E. U. Baranger, in *Advances in Nuclear Physics*, edi-

ted by M. Baranger (Plenum, New York, 1971), Vol. IV, Chap. 5, and references therein.

<sup>15</sup>L. S. Kisslinger and R. A. Sorenson, *Kgl. Danske Videnskab Selskab, Mat.-Fys. Medd.* **32**, No. 9 (1959); *Rev. Mod. Phys.* **35**, 853 (1963).

<sup>16</sup>R. Arvieu, *Ann. Phys.* **8**, 407 (1963); R. Arvieu, E. Baranger, M. Veneroni, M. Baranger, and V. Gillet, *Phys. Letters* **4**, 119 (1963).

<sup>17</sup>D. M. Clement and E. U. Baranger, *Nucl. Phys.* **A120**, 25 (1968), and references therein.

<sup>18</sup>M. Gmitro, A. Rimini, P. Rossi, and T. Weber, *Phys. Rev. C* **1**, 1801 (1970), and references therein.

<sup>19</sup>L. M. Bollinger, in *Proceedings of the International Meeting on Perspectives of Neutron Spectroscopy*, October 13-16, 1970, Dubna, USSR, to be published.

<sup>20</sup>A 2.8-g sample of  $^{115}\text{Sn}$  enriched to 30% (98% of the resulting radiation was due to capture in  $^{115}\text{Sn}$ ) was obtained from the Stable Isotope Sales Division, Oak Ridge National Laboratory.

<sup>21</sup>M. G. Strauss, I. S. Sherman, R. Brenner, S. J. Radnick, R. N. Larson, and H. M. Mann, *Rev. Sci. Instr.* **38**, 725 (1967); and private communication.

<sup>22</sup>N. S. Kendrick and D. A. McClure, to be published.

<sup>23</sup>J. B. Marion, *Nucl. Data A4*, 301 (1968).

<sup>24</sup>M. G. Strauss, F. R. Lenkszus, and J. J. Eichholz, *Nucl. Instr. Methods* **76**, 285 (1969).

<sup>25</sup>W. C. Davidon, Argonne National Laboratory Report No. ANL-5990 (Rev. 2) (unpublished).

<sup>26</sup>L. V. Groshev, B. I. Goavrilov, A. M. Domidov, *At. Energ. (USSR)* **6**, 281 (1959) [transl.: *Soviet J. At.*

Energy 6, 281 (1959)]; and J. Nucl. Energy 12A, 47 (1960).

<sup>26</sup>J. H. E. Mattauch, W. Thiele, and A. H. Wapstra, Nucl. Phys. 67, 1 (1965).

<sup>27</sup>Nuclear Data Sheets, compiled by K. Way *et al.* (Printing and Publishing Office, National Academy of Sciences-National Research Council, Washington, D.C.), NRC 60-3-105.

PHYSICAL REVIEW C

VOLUME 5, NUMBER 3

MARCH 1972

## Experiments on Parity Nonconservation in Nuclear Forces. III. Gamma Transitions in <sup>180</sup>Hf, <sup>159</sup>Tb, <sup>181</sup>Ta, <sup>203</sup>Tl, and <sup>182</sup>W<sup>†</sup>

E. D. Lipson, F. Boehm, and J. C. Vanderleeden\*  
California Institute of Technology, Pasadena, California 91109  
(Received 22 October 1971)

We have further studied the parity admixtures in nuclear  $\gamma$  transitions by measuring the circular polarization of  $\gamma$  rays from five nuclei with a technique different from that of our work I and II in this series. The experiments were performed with a forward-scattering rapidly reversing Compton polarimeter and a phase-sensitive detection system. The analyzing efficiency of the Compton polarimeter, including effects of multiple scattering, was determined by Monte Carlo calculations. It was necessary in most experiments to apply corrections for polarized bremsstrahlung associated with  $\beta$  decays. Calculations of bremsstrahlung effects were verified by experiments on <sup>198</sup>Au and <sup>177</sup>Lu. The residual asymmetry of the polarimeter itself was determined by control experiments on <sup>103</sup>Ru. The values of  $P_\gamma$  obtained were <sup>180</sup>Hf 501 keV,  $P_\gamma = (-23 \pm 6) \times 10^{-4}$ ; <sup>159</sup>Tb 363 keV,  $P_\gamma = (-1 \pm 5) \times 10^{-4}$ ; <sup>203</sup>Tl 279 keV,  $P_\gamma = (-0.04 \pm 0.10) \times 10^{-4}$ ; <sup>181</sup>Ta 482 keV,  $P_\gamma = (-0.031 \pm 0.025) \times 10^{-4}$ ; <sup>182</sup>W 1189 keV,  $P_\gamma = (-0.25 \pm 0.40) \times 10^{-4}$ . A survey and a discussion of these results is presented.

### I. INTRODUCTION

In two prior communications<sup>1,2</sup> (herein referred to as I and II) results were presented on measurements of the circular polarization of  $\gamma$  rays in <sup>181</sup>Ta, <sup>175</sup>Lu, <sup>203</sup>Tl, and <sup>75</sup>As. The observation of a net circular polarization was reported, supporting the presence of parity-nonconserving (PNC) nuclear forces as predicted by weak-interaction theories of the current-current form. The measurements had been performed with a Compton polarimeter using a technique of integrating the detector current. A specially designed switching pattern was used to suppress effects of drifts such as that due to source decay.

In this paper we report on studies of the nuclei <sup>159</sup>Tb and <sup>180</sup>Hf, a preliminary account of which has been communicated earlier,<sup>3</sup> as well as <sup>182</sup>W. These nuclei were chosen because of the presence of close-lying states of opposite parity which are expected to enhance the parity admixture. For comparison, measurements of the previously reported cases <sup>181</sup>Ta and <sup>203</sup>Tl were undertaken.

### II. EXPERIMENTAL CONSIDERATIONS

To analyze the  $\gamma$ -ray circular polarization a forward-scattering Compton polarimeter was

built. Just as in I and II, the statistical limitations were surmounted with an integral detection technique. In contrast to our earlier current-integration system, which used a complex switching pattern<sup>4</sup> at relatively low frequency to suppress drifts, the present system uses ac coupling and fast switching.

A block diagram of the system is given in Fig. 1. A 10-Hz reference sine wave from the lock-in amplifier (LIA) is converted into a square wave in the magnet control unit, controlling the power amplifier which in turn drives the forward-scattering magnet.  $\gamma$  rays reaching the detector after scattering in the magnet produce a detector current, which has dc and ac (10-Hz) components, the latter being a measure of circular polarization. The dc component is retained in the interface and the ac component is passed to the LIA which measures the amplitude of the in-phase 10-Hz component of the signal by synchronous demodulation. The output of the LIA is long-term averaged by means of a bipolar voltage-to-frequency converter and a pair of scalars which are read out every 100 sec onto a magnetic tape.

In Fig. 2 we show the Compton polarimeter.  $\gamma$  rays originating in the source material within the titanium capsule scatter off electrons in the inner region of the magnet and are detected by the coax-